Enhancement of Phase Dynamic Range in Design of Reconfigurable Metasurface Reflect Array Antenna Using Two Types of Unit Cells for E Band Communication

Daniel Rozban [1,*], Asaf Barom [1], Gil Kedar [2], Ariel Etinger [2], Tamir Rabinovitz [2] and Amir Abramovich [1]

[1] Department of Electrical and Electronic Engineering, Ariel University, Ariel 40700, Israel; asaf8040@gmail.com (A.B.); amir007@ariel.ac.il (A.A.)

[2] Ceragon Networks Ltd., Rosh Ha'ayin 4810002, Israel; gilke@ceragon.com (G.K.); ariele@ceragon.com (A.E.); tamirr@ceragon.com (T.R.)

[*] Correspondence: rozbandaniel@gmail.com

Abstract: The deployment of wireless communication networks in the E band (60–90 GHz) requires highly flexible, real-time, and precise tunability to optimize power transmission amidst diffraction, obstacles, and scattering challenges. This paper proposes an innovative reconfigurable metasurface reflect array design capable of achieving a dynamic phase range of 312 degrees with less than 1 dB of loss. The design integrates two types of unit cells and employs piezoelectric crystal as the tuning element. Simulation results illustrate the feasibility of beam focusing and accurate beam steering within a range of ±3 degrees. Furthermore, the proposed reconfigurable metasurface reflector demonstrates an antenna gain comparable to that of a dish antenna with the same aperture size.

Keywords: wireless communication; metasurface; intelligent reflection surface (IRS); millimeter wave (MMW); piezoelectric crystal

1. Introduction

A metasurface (MS) reflect array antenna comprises a feed and an array of reflecting elements, known as unit cells, arranged on a surface. Each unit cell can be tailored to reflect a specific phase shift, allowing for the generation of secondary radiation patterns [1–3]. These patterns encompass beam steering at a designated angle θ and the formation of a flat parabolic surface (FLAPS) [4].

Achieving beam steering at an angle θ involves applying a progressive phase shift to each unit cell of the metasurface. Figure 1 illustrates the typical configuration of a metasurface with an off-axis projection. According to Fresnel's law, the incident angle θi relative to the surface normal equals the reflection angle θr. The resulting steering angle θ is influenced by both θi and the designed metasurface steering angle [5].

In the FLAPS scenario, positioning the pyramidal horn antenna feed, as depicted in Figure 1, at the FLAPS's focal point generates a collimated beam. Additionally, utilizing this horn antenna to introduce a planar wave onto the FLAPS yields a focused beam.

According to the phased array theory, each unit cell location on the metasurface (MS) is defined at its center [6]. A 2D surface on the *XY* plane with a spatial array arrangement at a fixed distance and a 90° angle between the unit cells is denoted as $S(X_j, Y_i)$, where $j = 1, 2, \ldots, N$ and $i = 1, 2, \ldots, M$. Here, N and M are integer numbers, resulting in an array of $N \times M$ unit cells. This array, with the desired phase distribution throughout the surface, enables manipulation of the reflected wavefront pattern, such as focusing [7] or steering towards the desired direction [8].

A side cross-section view depicting the beam steering generated by the MS reflector is illustrated in Figure 2.
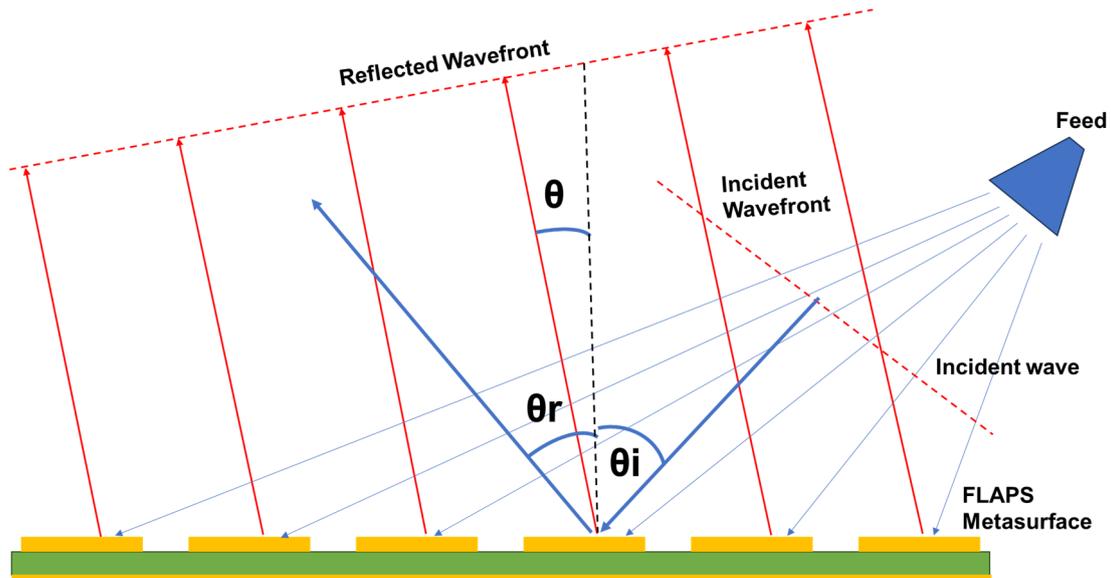
Figure 1. Configuration of the off-axis FLAPS metasurface integrated with a horn antenna feed. The steering of the incident wavefront is achieved by applying a progressive phase shift across the unit cells of the FLAPS metasurface.
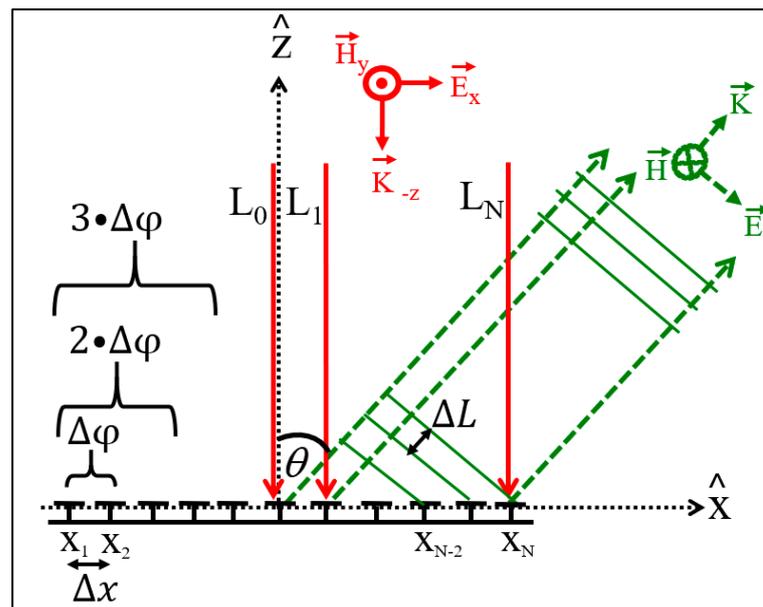
Figure 2. MS reflector lateral cross-section scheme of beam steering principle [4,5].

Figure 2 depicts a side-view schematic of wavefront steering by the MS reflect array antenna. The incident wavefront is represented by rays L_0, L_1, up to L_N. With each unit cell of the MS providing a predetermined gradual phase, the reflected rays (wavefront) are directed at the desired angle θ. The Optical Path Difference (OPD) between the reflected rays from unit cells X_j to X_{j+1} is defined as ΔL and is given by (1):

$$\Delta L = \Delta X \cdot sin\theta \tag{1}$$

where ΔX is the array periodicity of the MS. For beam steering, ΔL remains constant for all different paths from adjacent cells X_j and X_{j+1} throughout the MS. The conversion of ΔL into phase difference is depicted in Equation (2):

$$\Delta\varphi_x = \frac{360 \cdot \Delta L}{\lambda} \tag{2}$$

By introducing the phase difference $\Delta\varphi_x$ between adjacent unit cells X_j and X_{j+1} along the *X*-axis, a gradual accumulation of phase is achieved, resulting in the desired steering angle θ in the *XZ* plane, as depicted in Figure 2. Utilizing Equations (1) and (2), the desired steering angle θ is derived from $\Delta\varphi$ and ΔX, as outlined in Equation (3):

$$sin^{-1}\left(\frac{\lambda \cdot \Delta\varphi_x}{360 \cdot \Delta X}\right) \tag{3}$$

For the steering angle θ in the *YZ* plane, the analogous analysis applies by employing $\Delta\varphi y$ between adjacent unit cells along the *Y*-axis and ΔY in Equations (1)–(3).

Three-dimensional electromagnetic simulation software such as HFSS (2023 R2) and CST (2024.02) [9] can effectively simulate two-dimensional periodic structures. Dedicated solvers designed for these structures simplify the simulation process and save time by enabling the extraction of surface reflection properties and dispersion diagrams from a single-unit cell simulation [10]. In an MS reflect array antenna, the amplitude at each unit cell is determined by the wavefront pattern of the primary feed, allowing manipulation of only the phase at each unit cell of the MS. Whether employing pencil, shaped, or contoured wavefront patterns, local phase shifts are achieved by adjusting one or more geometrical parameters at each element. Reconfigurable MS reflect array antennas feature tuning elements capable of electrically shifting the reflected phase of each unit cell, facilitating fast and real-time tuning. The integration of tunable elements into MS unit cells enables a wide range of applications, including tuning beam-steering reflectors [11], reflective surfaces functioning as parabolic mirrors with adjustable focus [5,12], and more [13–16]. The ability to tune and reconfigure the reflected phase distribution throughout the MS reflector allows for beam steering (refer to Figure 1 and Equation (3)). This approach, known as phase-gradient, is divided into two sub-approaches: the quantization of the reflected phase shift of the unit cell into two values, four values, etc. [17], and the continuous reflected phase shift of the unit cell [11]. Various methods exist to incorporate tuning elements into an MS, such as PIN switches, MEMS switches, liquid crystal (LC) materials, piezoelectric materials, and varactor diodes. These methods are classified into three types: variations in material parameters, variations in the geometry, and circuit tuning.

Variations in material parameters comprising the MS reflect array can significantly affect the reflected phase shift of the unit cell. One widely utilized example is liquid crystal [18–21]. Liquid crystal materials consist of molecules that alter their polarization direction in response to an external DC voltage, thereby enabling control over the light intensity passing through the material and its refractive index.

Variations in the geometry of the unit cell itself or its dimensions also impact the tuning of MS properties. One example of such tuning elements is piezoelectric crystals and micro-electromechanical systems (MEMS). These elements facilitate continuous changes in the unit cell thickness in response to the DC voltage supplied to them [22–25]. Consequently, the electromagnetic properties of the MS undergo continuous alteration as well.

Circuit tuning is typically achieved using a varactor diode [3,4,11,26,27] for continuous adjustments or a PIN switch [28–30] for discrete adjustments. A varactor diode introduces tuning capacitance to the unit cell of the MS based on the reverse voltage applied to it. Conversely, a PIN switch facilitates ON/OFF operation, allowing for discrete adjustments of the unit cell. These tuning components play a crucial role in modifying the electromagnetic properties of the MS. Moreover, the response time of these diodes is exceptionally fast, typically on the order of nanoseconds. Additionally, they can be seamlessly integrated

into standard PCB circuits. If these tuning components are significantly smaller than the relevant wavelength, they can be simulated as lumped elements.

Achieving optimal performance of the MS reflect array antenna necessitates a 360° phase dynamic range. Additionally, the reflected magnitude across the entire phase dynamic range should remain uniform with minimal losses. However, no tuning elements or unit cell geometries can inherently provide the entire phase range with uniform, lossless magnitude. Consequently, once the phase distribution on the MS reflect array surface is determined, the optimization process for each element and unit cell of the MS is utilized to attain the required phase value with minimal losses. Furthermore, most reflect array unit cells and tuning elements are sensitive to the angle of incidence of the wavefront relative to the MS normal. This sensitivity can degrade the performance of the MS reflect array antenna. Therefore, a proper design process should account for the varying angles of incidence beams. One method to enhance the performance of reconfigurable MS reflect array antennas is the stripes method [31]. Based on this method, a Ku band MS reconfigurable reflect array antenna was designed with two types of tunable unit cells, type A and type B, arranged in three stripes on the reflect array surface, as depicted in Figure 3. The tuning element employed in this design was the varactor diode.
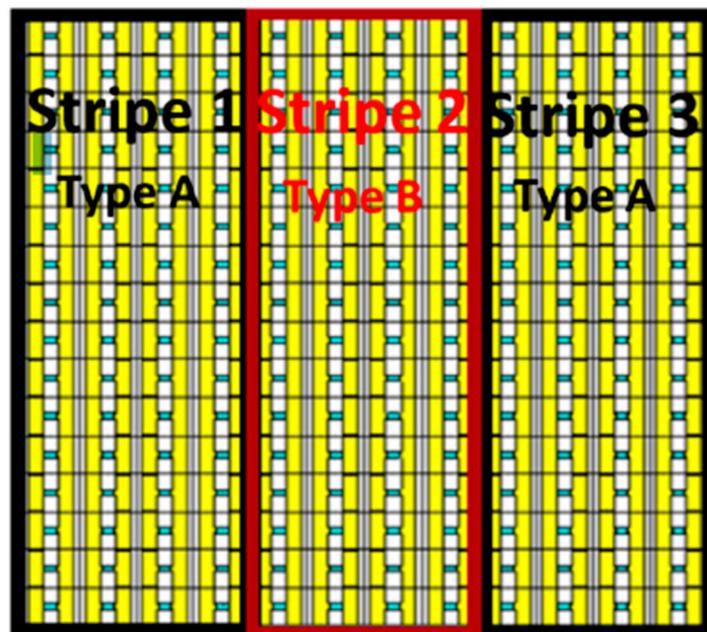
Figure 3. MS structure with three bands affixed to each other. Varactor diodes, identified by green rectangles, are prominently featured within the structure [31].

Each unit cell type, along with its varactor diode, was meticulously designed to achieve a reflection coefficient close to one across a portion of the entire phase dynamic range. This strategic design allowed the two types, arranged in stripes as depicted in Figure 3, to collectively possess a phase dynamic range very close to 360° with a reflection coefficient approaching unity. Simulation results of this design showcased a notable enhancement of 3 dB in antenna gain, contingent upon the steering angle. Moreover, a significant improvement of approximately 50% in steering angle accuracy for various operating frequencies was demonstrated [31].

Reflect array antennas offer several advantages compared to phased arrays and parabolic reflectors. Reflect arrays can provide high gain, precise and rapid scanning and steering, and low cross-polarization [1,2,32]. Additionally, reflect arrays boast low loss, ease of PCB manufacturing, and the potential for electronic control of the reflected wavefront pattern [1,2].

In this study, a novel concept of a reconfigurable MS reflect array antenna based on patch unit cells and piezoelectric crystal bending as a tuning element for E band (60–90 GHz) communication is proposed. The proposed reflect array comprises two types of unit cells, enabling a very large phase dynamic range of approximately 312° and a reflectance coefficient very close to one. As radiation at Millimeter wave (MMW) frequencies attenuate rapidly over distance, highly directional antennas are required to focus and direct their power [33]. Blockages or obstacles introduce variations in MMW path loss characteristics, with paths categorized as line-of-sight (LOS) and non-line-of-sight (non-LOS), necessitating real-time steering corrections of the antenna to optimize the channel [33]. Environmental factors such as winds can sway the reflector, leading to degradation of channel performance and requiring a real-time compensation mechanism [33]. This study presents and analyzes very accurate steering of ±3° and focusing with an antenna gain of about 30 dB. MMW wave steering can be electrically controlled by applying a control voltage to a piezoelectric crystal bender. The response time of the piezoelectric crystal bender is in the order of 1 μs, enabling the MS reflector to compensate for beam steering errors due to environmental influences such as winds.

2. Unit Cell and MS Design

The unit cell designed for the E band (60–90 GHz) regime is depicted in Figure 4. It is important to note that two parameters, Wp and g, are utilized to augment the phase dynamic range of the MS reflect array antenna while maintaining the reflectance coefficient close to one.
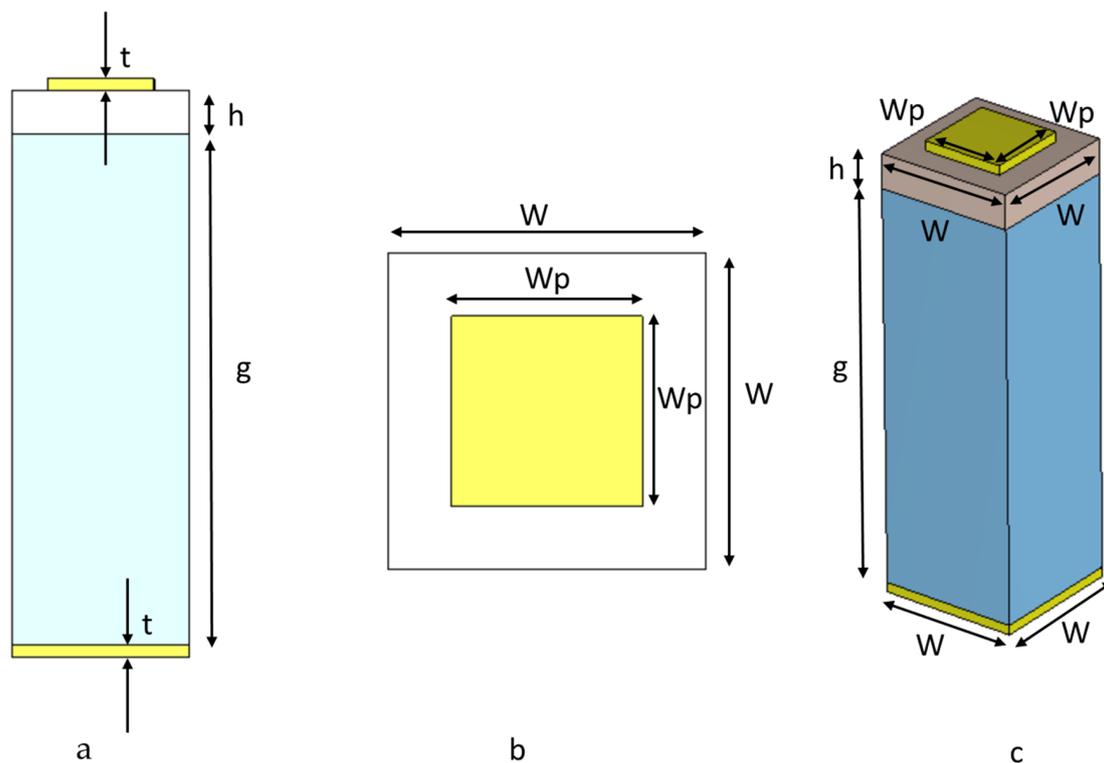
Figure 4. Unit cell design: (**a**) side view, (**b**) top view, (**c**) 3D view.

The unit cell size was selected to be W = 0.9 mm, slightly smaller than a quarter of the wavelength at a frequency of 80 GHz, thus qualifying it as a metasurface unit cell [1–5]. This unit cell comprises a ground surface with a copper thickness of t = 0.035 mm, an adjustable air gap, g, and a variable patch width, Wp, printed on a dielectric substrate with a thickness of h. To augment the phase dynamic range of the MS reflect array antenna, a methodology akin to the stripe method was employed [31]. Two distinct unit cell types were developed: type A with g = 1.95 mm and type B with g = 1.75 mm.

Rogers 5880 (*tanδ* = 0.0009, *εr* = 2.2) with a thickness of h = 0.252 mm was chosen as the dielectric substrate owing to its minimal losses and low relative permittivity [34]. Composed of PTFE composite substrates with woven glass reinforcement, Rogers 5880 can operate effectively up to millimeter-wave frequencies [34]. A W-band single-layer reflect array antenna based on this substrate was previously designed, fabricated, and measured at 94 GHz [32]. The design parameters employed in that study were obtained from the Rogers 5880 datasheet [34]. The consistency between the simulations and experimental results [32] validates these design parameters up to 115 GHz [34]. Consequently, an almost constant relative permittivity and loss tangent from low frequencies up to 115 GHz (and potentially beyond) is anticipated.

Figure 5 illustrates the phase dynamic range of the reflected beam as a function of the patch width, Wp, at 80 GHz. Two types of unit cells are displayed in Figure 5: the lower graph corresponds to type A with g = 1.95 mm, while the upper graph represents type B with g = 1.75 mm. Table 1 summarizes the design parameters of the unit cell and MS reflect array.
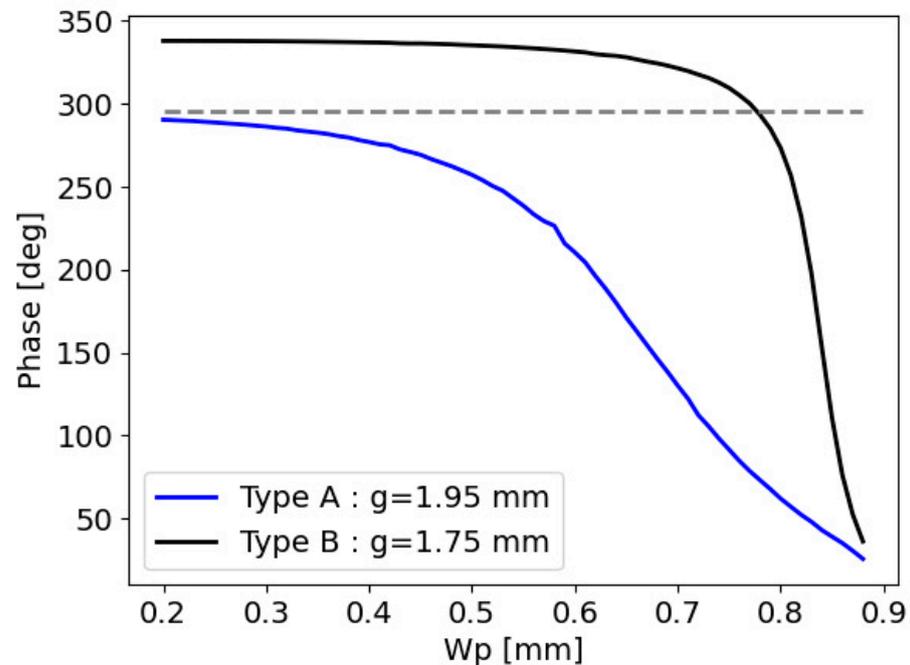
Figure 5. Reflected phase dynamic range of the unit cell as a function of the patch width, Wp. The lower graph corresponds to type A with g = 1.95 mm, while the upper graph represents type B with g = 1.75 mm.

Table 1. Parameters of the designed unit cell and metasurface reflector.

Parameters	Description	Value (mm)
W	Unit cell size	0.8
W_p	Patch size	Variable
t	Copper thickness	0.035
g	Air gap thickness	Type A: g = 1.95, type B: g = 1.75
h	Dielectric substrate thickness	0.254
D	Diameter of the reflector	80
F	Focal length of the reflector	80
f	Frequency	80 GHz

By employing two distinct types of unit cells, the dynamic range of the reflected phase is expanded while ensuring a reflectance coefficient close to one for all patch widths. This strategy leverages the unique characteristics of each unit cell type to accommodate different ranges of reflected phases. The transition phase between using type A and type B unit cells occurs at 290 degrees, as denoted by the dashed gray line in Figure 5. For reflected phases exceeding 290 degrees, unit cell type B is utilized, whereas unit cell type A is employed for reflected phases below this threshold. This approach significantly enhances the reflected phase dynamic range.

Another benefit of this method is the gradual adjustment of phase relative to the patch width. The MS reflect array antenna in this study was designed to focus an 80 GHz millimeter-wave beam using a combination of the described two types of unit cells. Additionally, the metasurface was configured with a circular aperture with a diameter of 80 mm. Thus, realizing such an MS reflect array antenna necessitates integrating thousands of unit cells, each with different parameters of Wp and g based on the phase requirements.

From a practical standpoint, designing such metasurfaces requires an algorithm capable of automatically generating thousands of unit cells with varying parameters. In this study, CST software was utilized to simulate both the unit cell and the entire MS reflect array antenna. While CST allows scripting in a programming language named VBA to construct complex surfaces, VBA language can be cumbersome for complex calculations. Therefore, we developed a Python script that generates a text file containing all the VBA commands necessary to build this optimized metasurface. Utilizing this script, one can design an MS reflect array antenna within the CST platform based on a few design parameters such as focal length *F*, aperture diameter *D*, unit cell size *W*, and frequency *f*. This unique algorithm employs a function called meshgrid on two axes, *x* and *y*, to position each unit cell at a fixed distance according to the unit cell period W. The phase dispersion as a function of the positions within the metasurface is calculated based on the optical path difference (OPD) as given in Equation (4).

$$\textbf{\textit{Phase}}\,(\textbf{\textit{x}},\textbf{\textit{y}}) = \left[\sqrt{x^2 + y^2 + F^2} - F \right] \cdot \frac{360}{\lambda} \tag{4}$$

where λ is the wavelength and *F* is the focal length of the reflector. In this study, the chosen frequency is 80 GHz, resulting in a wavelength of 3.75 mm. Additionally, the focal point *F* and the reflector diameter *D* were both set to 80 mm. The values of Wp and g for each unit cell position on the MS reflector were calculated based on the required phase correction given in Equation (4).

The simulation of the reflected phase of the unit cell was conducted using the Floquet method, with the simulation results depicted by the yellow graphs in Figure 6. The reflected phase of each MS unit cell is determined by the values of Wp and g. The black curves in Figure 6 were generated using an approximation function that determines the required patch width Wp for any desired phase reflection. This function also completes the required patch width Wp for phases that fall outside the phase range provided by the Floquet method simulation (yellow curves). The approximation function (black line) was utilized to position unit cells at any location (*x*, *y*) with the correct patch width Wp and gap g according to the required phase specified in Equation (4).

The phase correction applied to the reflected wave from the metasurface can be utilized to either focus or collimate a millimeter-wave (MMW) beam. A plane wave incident on the MS will be focused to the focal length *F*, while a wave emanating from the focal length will be collimated. Figure 6 (left) corresponds to unit cell type A, while Figure 6 (right) represents unit cell type B.
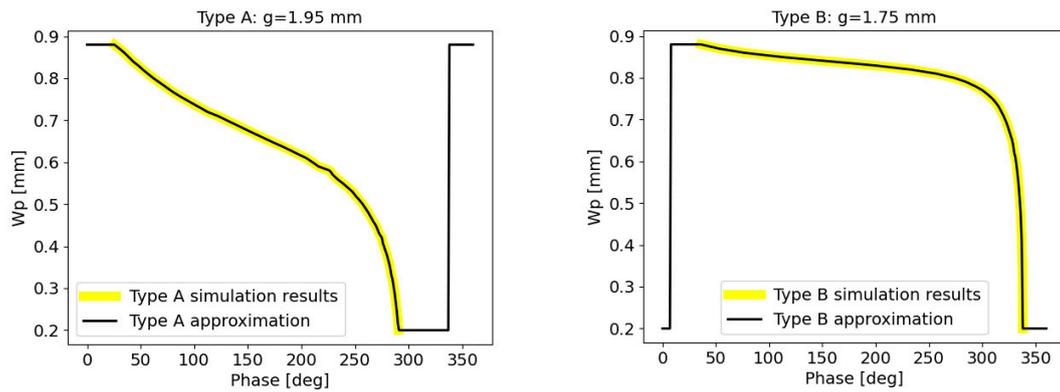
Figure 6. Unit cell reflected phase simulation conducted using the Floquet method. The yellow graphs represent the phase reflection as a function of the patch width, Wp, for unit cell type A (**left** graph) and unit cell type B (**right** graph). The black curves, generated by an approximation algorithm, provide additional insight into the relationship between phase reflection and patch width.

The simulation of the reflected magnitude of the unit cell using the Floquet method is depicted in Figure 7. The left graph corresponds to type A unit cells, while the right graph corresponds to type B unit cells. This simulation considers both the dielectric losses and the losses attributed to the final conductivity of the copper.
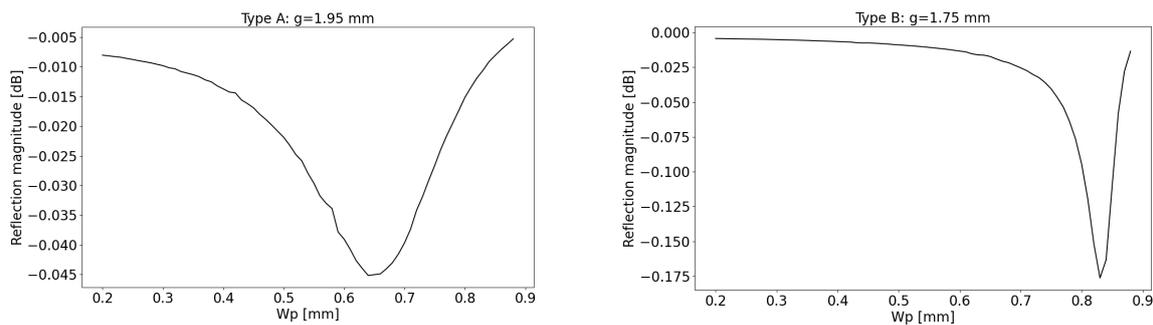
Figure 7. The unit cell reflected magnitude simulation based on the Floquet method. The (**left**) graph is for unit cell type A and the (**right**) is for unit cell type B.

The simulation results depicted in Figure 7 reveal that the losses of the designed metasurface are minimal. Moving to Figure 8, the MS reflector designed using the algorithm outlined above is showcased. On the right side of Figure 8, the metallic ground surface is displayed, featuring contours corresponding to unit cells type A and type B. Meanwhile, on the left side of Figure 8, the corresponding printed copper patches are shown. The varying sizes of these patches were computed based on Equation (4) and the approximation function depicted in Figure 6.

Piezoelectric benders, such as the Thorlabs PB4NB2W with a ±450 μm displacement capacity, can be utilized to rotate the metallic ground surface around its center, as demonstrated in the side view of the constructed MS reflector depicted in Figure 9. This rotation alters the gap distance between the metallic ground surface shown in Figure 8 (right) and the substrate with the copper patches depicted in Figure 8 (left). The gradual modification in the gap distance, denoted as g, for both type A and type B unit cells along the horizontal axis, induces a corresponding gradual change in the reflected phase of these unit cells, thereby influencing the deflection of the reflected beam.
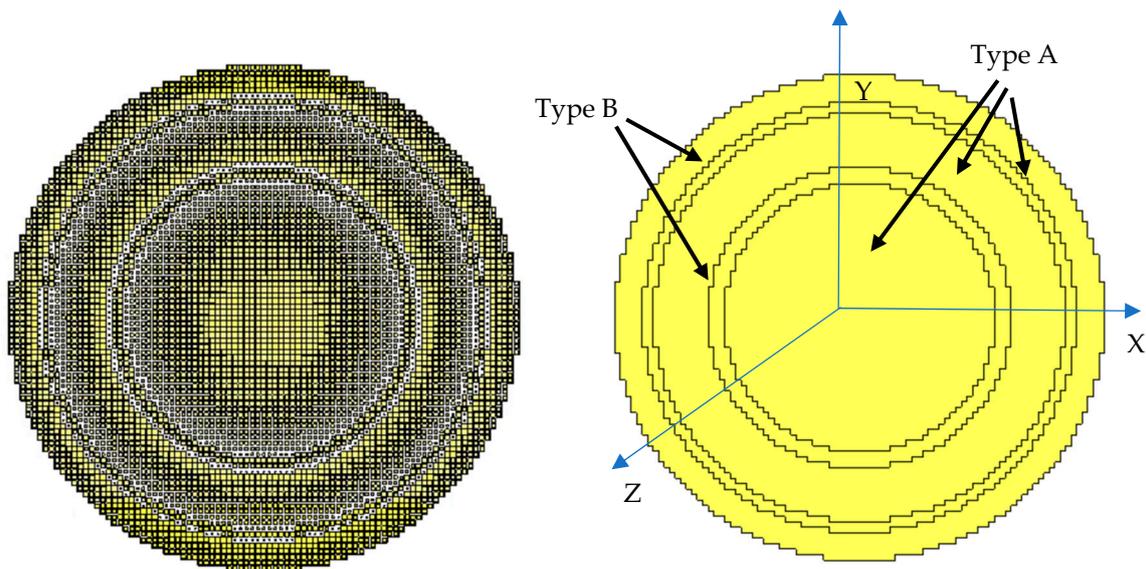
Figure 8. On the (**right**) side is the metal ground surface which includes contours of type A and type B, and on the (**left**) side is the substrate with different patch sizes according to the calculation of Equation (4).
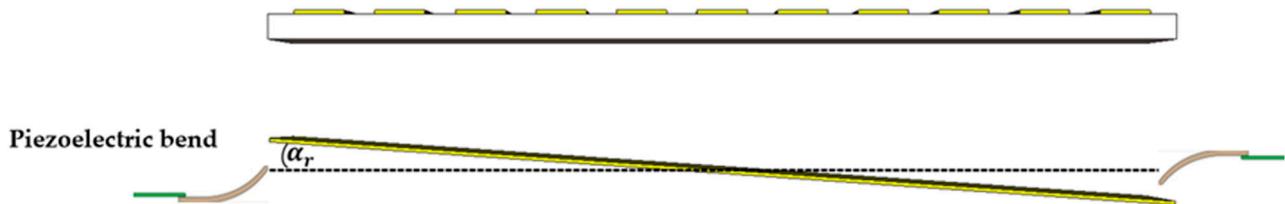
Figure 9. Side view of the MS structure with the piezoelectric bender.

3. Simulation Results

The outcome of the metasurface algorithm was simulated using CST to examine its focal point position along the Z-axis (see Figure 8). In the CST simulation, a plane wave illuminated the reflector, and Figure 10 displays the reflected electric field intensity as a function of distance on the Z-axis from this reflector. The maximum intensity of the reflected electric field was observed at approximately 75 mm from the center of the metasurface reflector, closely matching the designed value of 80 mm.

For comparison, a metallic three-dimensional parabolic reflector with the same focal length of 80 mm and the same diameter of 80 mm was also simulated using CST. The simulation result for this case showed a focal length of about 75 mm, which is nearly identical to that of the proposed metasurface reflector.

The directivity of the constructed MS reflector was simulated using a horn antenna positioned at the metasurface focal point. The simulation results are illustrated in Figure 11 for the cases of $\alpha_r = 0°$, $\alpha_r = 0.5°$ and $\alpha_r = 1°$ (see Figure 9).
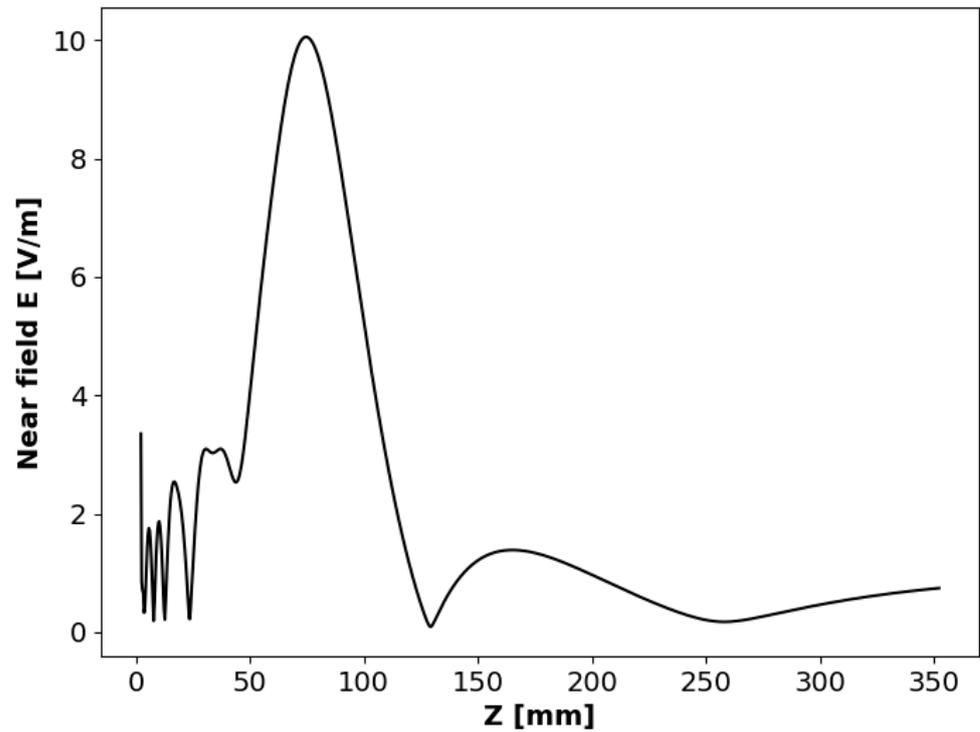
Figure 10. Electric field intensity as a function of distance from the metasurface. The simulation indicates that the focus is located approximately 75 mm from its center.
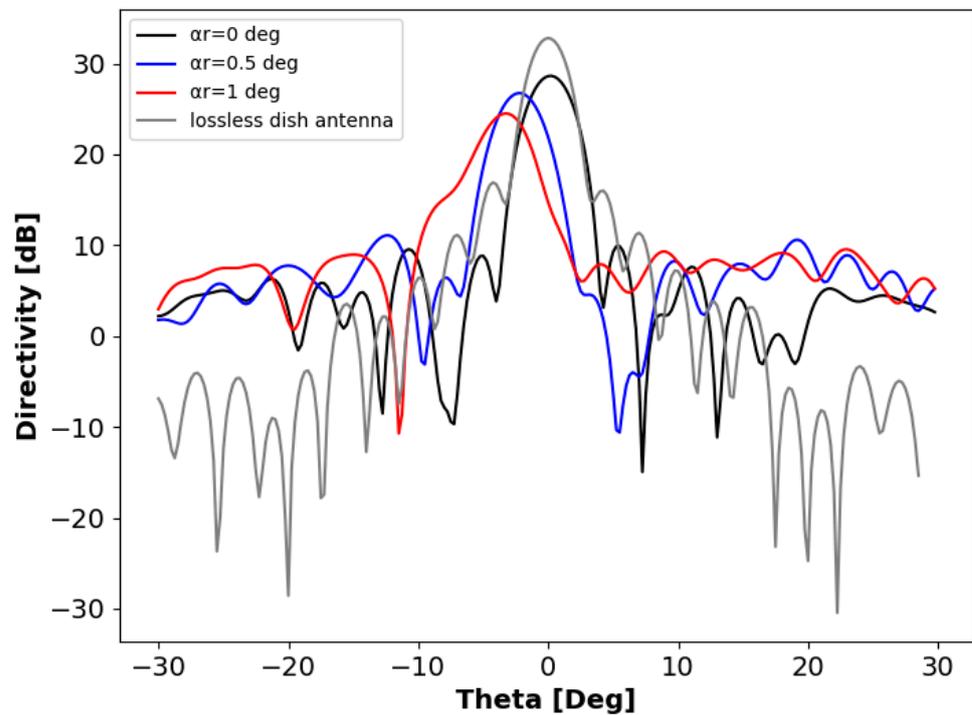
Figure 11. Simulation results of the constructed MS reflector directivity for three rotation angles: the first with $\alpha_r = 0$ (black line), the second with $\alpha_r = 0.5°$ (blue line), and the third with $\alpha_r = 1°$ (red line). The reflected beam steering for $\alpha_r = \pm 0.5°$ is approximately $\pm 2.25°$, and for $\alpha_r = \pm 1$, it is about $\pm 3°$. Additionally, a graph depicting an ideal parabolic antenna is included for reference.

The simulation results depicted in Figure 11 illustrate the beam steering capability of the proposed MS, ranging from $\theta = -3°$ to $\theta = +3°$ for rotation angle α_r between $-1°$ and

+1°. Each plot was taken with φ equal to 90 degrees. The described metasurface underwent simulation tests to assess its performance against varying plane wave incident angles and their effects. Figure 12 illustrates the simulation results for a plane wave radiating at angles of incidence of 1, 1.5, and 2 degrees.
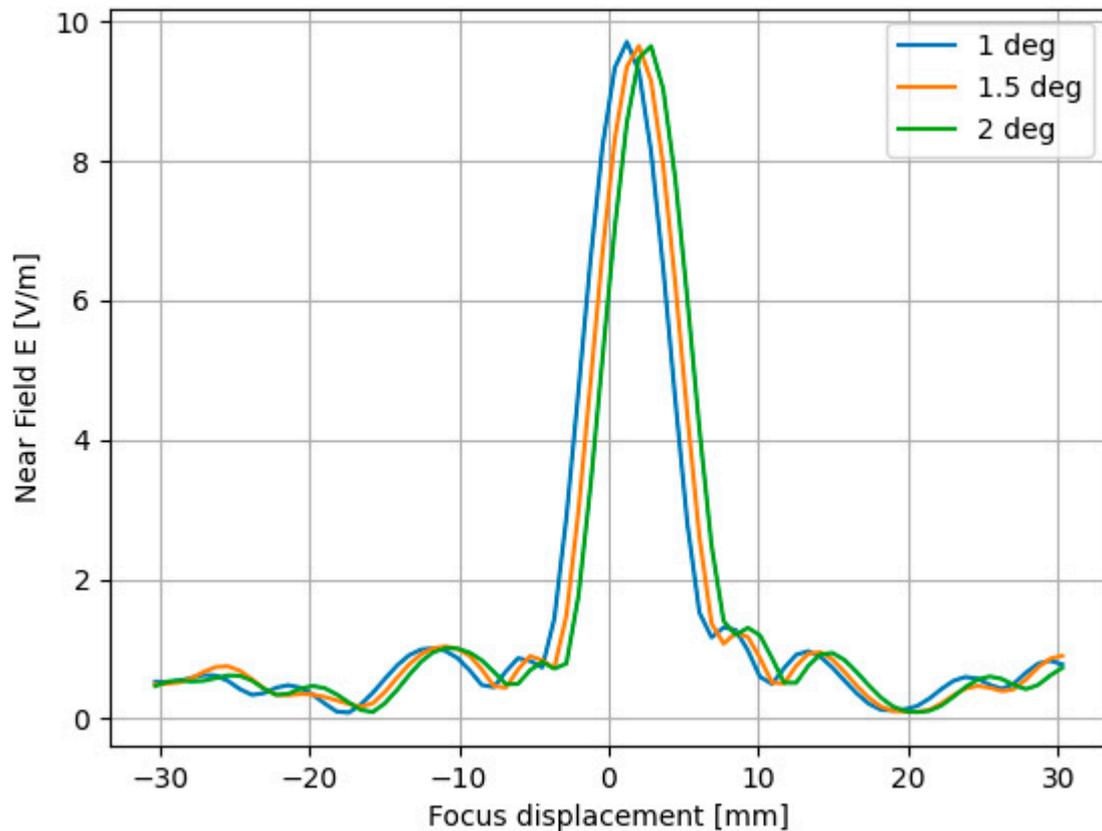
Figure 12. The simulation results of the displacement of the focal point from its origin (at the incident angle of 0 degrees) caused by the incident plane wave angle. The analysis encompasses incident angles of 1, 1.5, and 2 degrees.

The results depicted in Figure 12 demonstrate that the deviation of the incident wave angle indeed alters the focus position on the metasurface, as anticipated. However, despite these variations, the performance of the metasurface remained largely consistent across the tested angles. Furthermore, additional simulations were conducted to assess the impact of the wave frequency on the directivity of the metasurface. Remarkably, the directivity remained consistently high despite variations in the wave frequency. Table 2 compares the presented technology with other research works utilizing different technologies.

Examination of Table 1 highlights the advantages of the metasurface array designed in this study, including reduced attenuation, high gain, and cost-effectiveness. Notably, unlike alternative approaches outlined in references [35–37], our design streamlines the process by eliminating the need for individual diodes per unit cell and the requirement for precise voltage allocation to each diode or segment of the liquid crystal (LC) surface. This metasurface underwent simulation for 1D beam steering, achieving a maximum of 3 degrees of steering. However, further optimized design could facilitate additional progress by integrating an additional perpendicular piezoelectric bender, thus enabling 2D beam steering capabilities.

Table 2. Comparison of the proposed reflector's performance with other studies found in the literature.

Feature	Ref. [35]	Ref. [36]	Ref. [37]	This Work
Tuning technology	PIN	LC	PIN	Piezoelectric
Frequency (GHz)	73	78	78	80
Response time	nsec	sec	nsec	μs
Phase range	180°	---	180° ± 30°	312°
Gain (dBi)	16.8	25.1	---	>25
Aperture (mm)	32 × 32	---	54 × 27	Diameter of 80 mm
Losses (dB)	6.2 (per element)	>10 (per element)	2.7	<0.2
BW (GHz)	---	---	74–84	78–82
Steering range	±70°	±6°	±60°	±3°
1D/2D	2D	1D	1D	1D

4. Discussion

The simultaneous demonstration of beam steering and focusing, as depicted in Figures 10 and 11, presents a compelling proposition for the deployment and alignment of wireless communication networks. The swift and remote alignment of the MS (metasurface) reflector contrasts favorably with traditional dish antennas. This capability confers notable advantages in terms of flexibility, efficiency, and ease of deployment across diverse communication scenarios. Moreover, as illustrated in Figures 12 and 13, minor alterations in the angle of the wave incident on the metasurface or slight shifts in wave frequency exert only a modest influence on the metasurface's performance concerning focal distance and directivity. The dynamic steering range of the constructed MS reflector spans ±3° degrees, achieved through piezoelectric benders rotating the metal ground from $\alpha_r = -1°$ to $\alpha_r = +1°$. The MS reflector exhibits a directivity of approximately 25 dB at $\theta = 3°$, a performance closely resembling that of a conventional dish antenna. Figure 13 illustrates the simulation results depicting the directivity of the fabricated metasurface reflector across various beam frequencies, compared to that of an ideal dish.
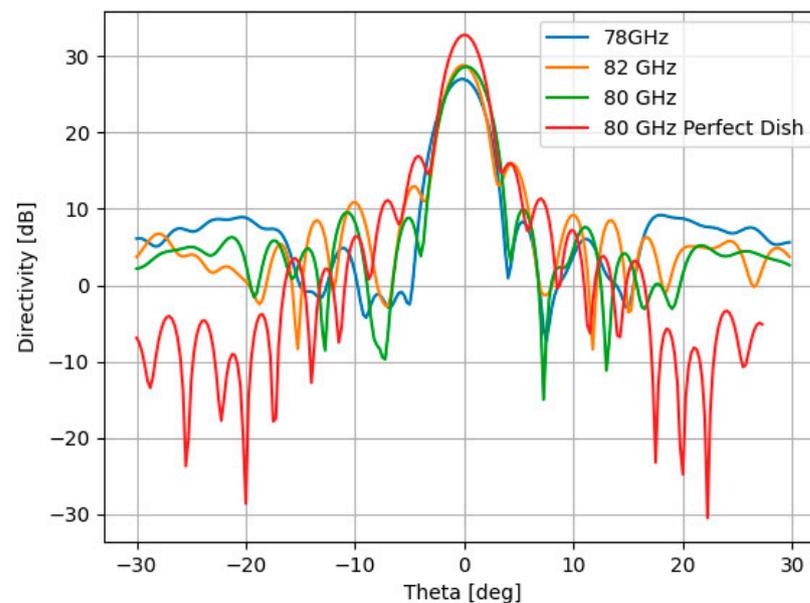
Figure 13. Presents the simulation results illustrating the directivity of the constructed MS (metasurface) reflector across various beam frequencies, compared with a perfect dish.

Additionally, a unique algorithm was devised for constructing the MS reflector, utilizing specific design parameters detailed in Table 1, such as diameter (D), frequency (f), focal distance (F), and the predefined unit cell. This algorithm has been thoroughly validated for

correctness and accuracy. Notably, the constructed MS comprises approximately 7000 unit cells of varying Wp sizes, arranged across approximately 50 contours and divided into 2 types of unit cells.

5. Conclusions

This article validates the concept of the stripe method, employing two types of unit cells to expand the dynamic range of the reflected phase. Furthermore, a unique algorithm was developed to construct the MS reflector based on these two types of unit cells. This algorithm demonstrated high efficiency, and the simulation results of the constructed MS reflector closely aligned with the theoretical principles of reflect arrays and dish antennas. The constructed MS reflector offers the dual capability of precisely focusing radiation onto the desired focal point and dynamically steering the reflected radiation within a range of $\pm 3°$ degrees.

Author Contributions: Investigation, D.R., A.B. and A.E.; Software, D.R. and T.R.; Research methodology, G.K., A.E. and T.R.; Conceptualization, A.B., A.E. and A.A.; Writing—original draft, D.R. and A.A.; Validation, T.R.; Supervision, A.A. All authors have read and agreed to the published version of the manuscript.

Funding: This research was funded by the Israel Innovation Authority, grant number "File 74724".

Data Availability Statement: Data are contained within this article.

Acknowledgments: We extend our gratitude to Ariel Scientific Innovations Ltd., Ariel University, Ceragon Networks Ltd.

Conflicts of Interest: Author Gil Kedar, Ariel Etinger, and Tamir Rabinovitz were employed by the company Ceragon Networks Ltd. The remaining authors declare that the research was conducted in the absence of any commercial or financial relationships that could be construed as a potential conflict of interest.

References

1. Dahri, M.H.; Jamaluddin, M.H.; Abbasi, M.I.; Kamarudin, M.R. A Review of Wideband Reflectarray Antennas for 5G Communication Systems. *IEEE Access* **2017**, *5*, 17803–17815. [CrossRef]
2. Roederer, A.G. Reflect array antennas. In Proceedings of the 2009 3rd European Conference on Antennas and Propagation, Berlin, Germany, 23–27 March 2009; pp. 18–22.
3. Rothschild, D.; Rahamim, E.; Abramovich, A. Innovative Reconfigurable Metasurface 2-D Beam-Steerable Reflector for 5G Wireless Communication. *Electronics* **2020**, *9*, 1191. [CrossRef]
4. Litmanovitch, G.; Rrotshild, D.; Abramovich, A. Flat mirror for millimeter-wave and terahertz imaging systems using an inexpensive metasurface. *Chin. Opt. Lett.* **2017**, *15*, 011101. [CrossRef]
5. Rothschild, D.; Abramovich, A. Wideband reconfigurable entire Ku-band metasurface beam-steerable reflector for satellite communications. *IET Microw. Antennas Propag.* **2019**, *13*, 334–339. [CrossRef]
6. Bhattacharyya, A.K. *Phased Array Antennas: Floquet Analysis, Synthesis, BFNs, and Active Array Systems*; John Wiley & Sons: Hoboken, NJ, USA, 2006; Volume 179.
7. Wang, Z.; Liao, D.; Zhang, T.; Chen, T.; Ruan, Y.; Zheng, B. Metasurface-based focus-tunable mirror. *Opt. Express* **2019**, *27*, 30332–30339. [CrossRef] [PubMed]
8. Vásquez-Peralvo, J.A.; Fernández-González, J.M.; Rigelsford, J.M. Beam Steering Using Active Artificial Magnetic Conductors: A 10-Degree Step Controlled Steering. *IEEE Access* **2020**, *8*, 177964–177975. [CrossRef]
9. Rütschlin, M.; Wittig, T.; Iluz, Z. Phased antenna array design with CST STUDIO SUITE. In Proceedings of the 2016 10th European Conference on Antennas and Propagation (EuCAP), Davos, Switzerland, 10–15 April 2016; IEEE: Piscataway, NJ, USA, 2016; pp. 1–5.
10. Ghasemifard, F.; Norgren, M.; Quevedo-Teruel, O. Dispersion analysis of 2-D glide-symmetric corrugated metasurfaces using mode-matching technique. *IEEE Microw. Wirel. Compon. Lett.* **2017**, *28*, 1–3. [CrossRef]
11. Sievenpiper, D.F.; Schaffner, J.H.; Song, H.J.; Loo, R.Y.; Tangonan, G. Two-dimensional beam steering using an electrically tunable impedance surface. *IEEE Trans. Antennas Propag.* **2003**, *51*, 2713–2722. [CrossRef]
12. Nadeem, M.; Shoaib, N.; Raza, A.; Saeed, W.; Shoaib, I.; Shoaib, S. 2-Dimensional (2D) Beam Steering-Antenna Using Active PRS for 5G Applications. *Micromachines* **2023**, *14*, 110. [CrossRef]
13. Li, A.; Singh, S.; Sievenpiper, D. Metasurfaces and their applications. *Nanophotonics* **2018**, *7*, 989–1011. [CrossRef]
14. Bukhari, S.S.; Vardaxoglou, J.Y.; Whittow, W. A metasurfaces review: Definitions and applications. *Appl. Sci.* **2019**, *9*, 2727. [CrossRef]

15. Faenzi, M.; Minatti, G.; González-Ovejero, D.; Caminita, F.; Martini, E.; Della Giovampaola, C.; Maci, S. Metasurface antennas: New models, applications and realizations. *Sci. Rep.* **2019**, *9*, 10178. [CrossRef]
16. Turpin, J.P.; Bossard, J.A.; Morgan, K.L.; Werner, D.H.; Werner, P.L. Reconfigurable and tunable metamaterials: A review of the theory and applications. *Int. J. Antennas Propag.* **2014**, *2014*, 429837. [CrossRef]
17. Yang, H.H.; Xu, L.M.; Yang, F.; Cao, X.Y.; Xu, S.H.; Gao, J.; Li, S.J. Phase quantization effects of coded metasurface on agile scattering field control. *Microw. Opt. Technol. Lett.* **2017**, *59*, 738–743. [CrossRef]
18. Ting, T.L. The technology of liquid crystal-based antenna. *Opt. Express* **2019**, *27*, 17138–17153. [CrossRef] [PubMed]
19. Yaghmaee, P.; Karabey, O.H.; Bates, B.; Fumeaux, C.; Jakoby, R. Electrically tuned microwave devices using liquid crystal technology. *Int. J. Antennas Propag.* **2013**, *2013*, 824214. [CrossRef]
20. Maune, H.; Jost, M.; Reese, R.; Polat, E.; Nickel, M.; Jakoby, R. Microwave liquid crystal technology. *Crystals* **2018**, *8*, 355. [CrossRef]
21. Foo, S. Liquid-crystal-tunable metasurface antennas. In Proceedings of the 2017 11th European Conference on Antennas and Propagation (EUCAP), Paris, France, 19–24 March 2017; IEEE: Piscataway, NJ, USA, 2017; pp. 3026–3030.
22. Momeni Hasan Abadi, S.M.A.; Booske, J.H.; Behdad, N. MAcro-Electro-Mechanical Systems (MÆMS) based concept for microwave beam steering in reflectarray antennas. *J. Appl. Phys.* **2016**, *120*, 054901. [CrossRef]
23. Mavridou, M.; Feresidis, A.P. Dynamically reconfigurable high impedance and frequency selective metasurfaces using piezoelectric actuators. *IEEE Trans. Antennas Propag.* **2016**, *64*, 5190–5197. [CrossRef]
24. Vassos, E.; Churm, J.; Feresidis, A. Ultra-low-loss tunable piezoelectric-actuated metasurfaces achieving 360° or 180° dynamic phase shift at millimeter-waves. *Sci. Rep.* **2020**, *10*, 15679. [CrossRef]
25. Asgharian, R.; Zakeri, B.G.; Yazdi, M. A Narrow Beam, Beam Steerable, and Low Side-Lobe Reflectarray Based on Macro Electro-Mechanical Technique. *Prog. Electromagn. Res.* **2020**, *100*, 73–82. [CrossRef]
26. Nie, J.; Tan, Y.Q.; Ji, C.L.; Liu, R.P. Analysis of Ku-Band steerable metamaterials reflect with tunable varactor diodes. In Proceedings of the 2016 Progress in Electromagnetic Research Symposium (PIERS), Shanghai, China, 8–11 August 2016; IEEE: Piscataway, NJ, USA, 2016; pp. 709–713.
27. Rotshild, D.; Abramovich, A. Realization and validation of continuous tunable metasurface for high resolution beam steering reflector at K-band frequency. *Int. J. RF Microw. Comput.-Aided Eng.* **2021**, *31*, e22559. [CrossRef]
28. Cui, T.J.; Qi, M.Q.; Wan, X.; Zhao, J.; Cheng, Q. Coding metamaterials, digital metamaterials and programmable metamaterials. *Light. Sci. Appl.* **2014**, *3*, e218. [CrossRef]
29. Amri, M.M.; Tran, N.M.; Park, J.H.; Kim, D.I.; Choi, K.W. A Programmable Binary Metasurface for Wireless Power Transfer Application. In Proceedings of the 2020 IEEE Wireless Power Transfer Conference (WPTC), Seoul, Republic of Korea, 15–19 November 2020; IEEE: Piscataway, NJ, USA, 2020; pp. 334–337.
30. Huang, C.; Sun, B.; Pan, W.; Cui, J.; Wu, X.; Luo, X. Dynamical beam manipulation based on 2-bit digitally-controlled coding metasurface. *Sci. Rep.* **2017**, *7*, 42302. [CrossRef] [PubMed]
31. Rahamim, E.; Rotshild, D.; Abramovich, A. Performance Enhancement of Reconfigurable Metamaterial Reflector Antenna by Decreasing the Absorption of the Reflected Beam. *Appl. Sci.* **2021**, *11*, 8999. [CrossRef]
32. Wang, Z.; Zhang, R.; Song, W.; Lin, X.; Xie, B.; Wang, J.; Zhao, R. W-Band Single-Layer Broadband Reflectarray Antenna. *IEEE Access* **2023**, *11*, 66309–66317. [CrossRef]
33. Peng, Z.; Li, L.; Wang, M.; Zhang, Z.; Liu, Q.; Liu, Y.; Liu, R. An effective coverage scheme with passive-reflectors for urban millimeter-wave communication. *IEEE Antennas Wirel. Propag.* **2015**, *15*, 398–401. [CrossRef]
34. Available online: https://www.rogerscorp.com/advanced-electronics-solutions/rt-duroid-laminates/rt-duroid-5880-laminates (accessed on 3 May 2024).
35. Liu, C.; Yang, F.; Xu, S.; Li, M. An E-Band Reconfigurable Reflectarray Antenna Using p-i-n Diodes for Millimeter-Wave Communications. *IEEE Trans. Antennas Propag.* **2023**, *71*, 6924–6929. [CrossRef]
36. Bildik, S.; Dieter, S.; Fritzsch, C.; Menzel, W.; Jakoby, R. Reconfigurable folded reflectarray antenna based upon liquid crystal technology. *IEEE Trans. Antennas Propag.* **2015**, *63*, 122–132. [CrossRef]
37. Sahoo, D.K.; Chakraborty, C.; Ruchi; Kundu, D.; Patnaik, A.; Chakraborty, A. A 1-Bit Coding Reconfigurable Metasurface Reflector for Millimeter Wave Communications in E-Band. In Proceedings of the 2023 IEEE Microwaves, Antennas, and Propagation Conference (MAPCON), Ahmedabad, India, 10–14 December 2023; pp. 1–4. [CrossRef]